

EXPLOSIVE NUCLEOSYNTHESIS IN ASPHERICAL HYPERNOVA EXPLOSIONS AND LATE TIME SPECTRA OF SN1998BW

KEIICHI MAEDA¹, TAKAYOSHI NAKAMURA¹, KEN'ICHI NOMOTO^{1,5}, PAOLO A. MAZZALI^{2,5}, FERDINANDO PATAT³, IZUMI HACHISU⁴

To appear in the January 2002 issue of ApJ (Vol. 565)

ABSTRACT

Aspherical explosion models for the hypernova (hyper-energetic supernova) SN 1998bw are presented. Nucleosynthesis in aspherical explosions is examined with a two-dimensional hydrodynamical code and a detailed nuclear reaction network. Aspherical explosions lead to a strong α -rich freezeout, thus enhancing the abundance ratios [⁴⁴Ca, ⁴⁸Ti, and ⁶⁴Zn / Fe] in the ejecta. The nebular line profiles of the Fe-dominated blend near 5200 Å and of [O I] 6300,6363 Å are calculated and compared with the observed late time spectra of SN 1998bw. Compared with the spherical model, the unusual features of the observed nebular spectra can be better explained if SN 1998bw is a strongly aspherical explosion with a kinetic energy of $\sim 10^{52}$ ergs viewed from near the jet direction.

Subject headings: supernovae: individual: SN1998bw — gamma rays: bursts — nucleosynthesis — line: profiles

1. INTRODUCTION

The exceptionally bright Type Ic supernova (SN Ic) SN 1998bw was discovered as the probable optical counterpart of the gamma-ray burst GRB980425 (Galama et al. 1998). The early light curve and the spectra of SN 1998bw have been successfully modeled as the hyper-energetic explosion (kinetic energy $E \sim 4 \times 10^{52}$ ergs) of a massive C+O star (Iwamoto et al. 1998; Woosley et al. 1999; Branch 2001). In this paper the term "hypernova" is used to refer to a SN explosion with $E \gtrsim 10^{52}$ ergs, regardless of the nature of the central engine (Nomoto et al. 2001a).

Despite the success of the hypernova model in reproducing the observed features of SN 1998bw at early times, some properties of the observed light curve and spectra at late times are difficult to explain. (1) The tail of the observed light curve declines more slowly than the synthetic curve, indicating that at advanced epochs γ -ray trapping is more efficient than expected (Nakamura et al. 2001a; Sollerman et al. 2000). (2) In the nebular epoch, the [O I]6300Å emission is narrower than the emission near 5200Å. As discussed in Mazzali et al. (2001), this latter feature is mostly due to a blend of [Fe II] lines. Mazzali et al. (2001) calculated synthetic nebular-phase spectra of SN 1998bw using a spherically symmetric NLTE nebular code based on the deposition of γ -rays from ⁵⁶Co decay in a nebula of uniform density and composition. They showed that the [O I] and the [Fe II] features can only be reproduced if different velocities are assumed for the two elements. A significant amount of slowly-moving O is therefore necessary to explain the profile of the [O I] line.

Both these features are in conflict with what is expected from a spherically symmetric explosion model, where γ -ray

deposition decreases with time and where iron is produced in the deepest layers and thus has a lower average velocity than oxygen. Mazzali et al. (2001) suggested that these are signatures of asymmetry in the ejecta. Therefore in this paper we examine aspherical explosion models for hypernovae.

Aspherical explosions of massive stars have been investigated as possible sources of gamma-ray bursts (GRBs) (Woosley 1993; Paczynski 1998). MacFadyen & Woosley (1999) showed numerically that the collapse of a rotating massive core can form a black hole with an accretion disk, while a jet emerges along the rotation axis. The jet produces a highly asymmetric explosion (Khokhlov et al. 1999). However, these studies did not calculate explosive nucleosynthesis, nor did they show spectroscopic and photometric features of aspherical explosions. Nagataki (2000) performed nucleosynthesis calculations for aspherical SN explosions to explain some features of SN 1987A, but he only addressed the case of a normal explosion energy.

In the present study, we examine the effect of aspherical explosions on nucleosynthesis in hypernovae. We then investigate the degree of asphericity in the ejecta of SN 1998bw, which is critically important information to confirm the SN/GRB connection, by computing synthetic spectra for the various models viewed with different orientations and comparing the results with the observed late time spectra of SN 1998bw (Patat et al. 2001).

2. ASYMMETRIC EXPLOSION MODELS

The first step of our calculation is the hydrodynamical simulation of the explosion with a 2D Eulerian hydrody-

¹Department of Astronomy, School of Science, University of Tokyo, Bunkyo-ku, Tokyo 113-0033, Japan

²Osservatorio Astronomico di Trieste, via G. B. Tiepolo 11, I-34131 Trieste, Italy

³European Southern Observatory, K. Schwarzschild Str. 2, D-85748 Garching, Germany

⁴Department of Earth Science and Astronomy, College of Arts and Science, University of Tokyo, Meguro-ku, Tokyo 153-0041, Japan

⁵Research Center for the Early Universe, School of Science, University of Tokyo, Bunkyo-ku, Tokyo 113-0033, Japan

emails: maeda@astron.s.u-tokyo.ac.jp, nakamura@astron.s.u-tokyo.ac.jp, nomoto@astron.s.u-tokyo.ac.jp, mazzali@ts.astro.it, fpatat@eso.org, hachisu@chianti.c.u-tokyo.ac.jp

namical code based on Roe’s scheme (Hachisu et al. 1992, 1994). Euler’s equations are solved with a constant adiabatic index $\gamma = 4/3$, which is a good approximation if the pressure is radiation-dominated. The effect of nuclear reactions on the hydrodynamics is negligible since the explosion energy is large. We use 120×120 meshes on a cylindrical (r, z) coordinate system. The mesh size is linearly zoned and decreases inward, which gives a high resolution of the hydrodynamic evolution of the central regions where explosive nucleosynthesis takes place. We follow 190 test particles initially in the C+O layer and 2250 particles initially in the Si layer and track their density and temperature histories. These histories are then used to calculate the change in the chemical composition, using a reaction network including 222 isotopes up to ^{71}Ge (Thielemann et al. 1996).

We construct several asymmetric explosion models for various combinations of the model parameters (Table 3). We use as progenitor the $16 M_{\odot}$ He core of a $40 M_{\odot}$ star (Nomoto & Hashimoto 1988). This has a $13.8 M_{\odot}$ C+O core, the same as that used in Iwamoto et al. (1998). We test three values of the final kinetic energy: $E = 1 \times 10^{51}$, 1×10^{52} , and 3×10^{52} ergs. The hydrodynamical simulation is started by depositing the energy below the mass cut that divides the ejecta from the collapsing core. The energy deposited is divided between thermal and kinetic energy, with various ratios. The asymmetry is generated by distributing the initial kinetic energy in an axisymmetric way. This is done by imposing different initial velocities in different directions: $v_z = \alpha z$ in the jet direction and $v_r = \beta r$ on the equatorial plane. The ratio α/β ranges from 16:1 to 1:1 (spherical case). The mass cut is set at $M_r = 2.4 M_{\odot}$, so that the ejected mass of ^{56}Ni is $\sim 0.4 M_{\odot}$ to reproduce the peak of the light curve (Nakamura et al. 2001a) in models A, B, C, E, and F.

3. NUCLEOSYNTHESIS

Figure 1 and 2 show respectively the post-shock peak temperatures and densities for the asymmetric hypernova model C in the direction of the jet and perpendicular to it (with those for the spherically symmetric hypernova model F also shown for comparison), and the isotopic composition of the ejecta of model C. In the z -direction, where the ejecta carry more kinetic energy, the shock is stronger and post-shock temperatures are higher, so that explosive nucleosynthesis takes place in more extended, lower density regions compared with the r -direction. Therefore, larger amounts of α -rich freeze-out elements, such as ^4He and ^{56}Ni (which decays into ^{56}Fe via ^{56}Co) are produced in the z -direction than in the r -direction. Also, the expansion velocity of newly synthesized heavy elements is much higher in the z -direction. The velocity of elements ejected in the z -direction in model C is actually similar to the result of a spherical explosion with $E \sim 3 \times 10^{52}$ ergs (Nakamura et al. 2001b), although the integrated kinetic energy is only $E = 1 \times 10^{52}$ ergs.

In contrast, along the r -direction ^{56}Ni is produced only in the deepest layers, and elements ejected in this direction are mostly the product of hydrostatic nuclear burning (O), with some explosive oxygen-burning products (Si, S, etc). The expansion velocities are much lower than in the z -direction.

Figure 3 shows the 2D distribution of ^{56}Ni and ^{16}O in model C in the homologous expansion phase. Near the z -axis the shock is stronger and a low density, ^4He -rich region is produced. ^{56}Ni is distributed preferentially in this direction, but it is mostly located slightly off of it because the shock propagates laterally as it penetrates the stellar envelope. As a result, the distribution of heavy elements is elongated in the z -direction, while that of ^{16}O is less aspherical. On the other hand, because the ejecta move more slowly in the r -direction, densities in this direction are higher than in the z -direction.

Tables 1 and 2 give respectively the detailed yields and the abundances of major stable isotopes relative to the solar values for model C (in Table 2, $[A/B] \equiv \log_{10}(A/B) - \log_{10}(A/B)_{\odot}$, where A and B are nuclear mass fractions). The main characteristics can be summarized as follows (see also Nomoto et al. 2001b).

(1) The complete Si-burning region is more extended for larger explosion energies. The aspherical explosion causes a region of higher entropy along the z -axis, which offers better conditions for the α -rich freezeout (Fig. 1). The high entropy inhibits the production of ^{56}Ni . Much ^4He is left after the freezeout, so that the elements produced through ^4He capture are very abundant in the deepest region along the z -axis (Fig. 2). This results in the enhancement of the elements synthesized in the deepest region, such as ^{44}Ca (produced as ^{44}Ti), ^{48}Ti (as ^{48}Cr), and elements heavier than $A \sim 58$. Because of the enhancement of these elements and the simultaneous suppression of ^{56}Ni , the abundances of these elements relative to iron (e.g., $[^{44}\text{Ca}, ^{48}\text{Ti}, ^{64}\text{Zn}/\text{Fe}]$) are greatly enhanced. For more asymmetric explosion, the effect of α -rich freezeout is even larger.

(2) Incomplete Si-burning and O-burning regions are more extended for larger explosion energies (Nakamura et al. 2001b). This results in the enhancement of ^{28}Si , ^{32}S , ^{40}Ca , ^{52}Cr (produced as ^{52}Fe), ^{54}Fe , and in the reduction of O. Asphericity has little effect on the production of these elements.

The most pronounced effect of asphericity is that elements produced by the strong α -rich freezeout are greatly enhanced relative to iron (e.g., $[\text{Ti}/\text{Fe}]$). For other explosive burning products, the effect of a large explosion energy usually dominates over that of asphericity.

4. THE LATE TIME SPECTRA OF SN 1998BW

In order to verify the observable consequences of an axisymmetric explosion, we calculated the profiles of the $[\text{Fe II}]$ blend and of $[\text{O I}]$ for models A-G. Line emissivities were obtained from a 1D NLTE nebular code (Mazzali et al. 2001), and the column densities of the various elements along different lines of sight were derived from the element distribution obtained from our 2D explosion models. Because we assume that the nebula is optically thin, the blended nature of the emissions is automatically taken into account.

These are compared to the 26 Nov 1998 spectrum of SN 1998bw. We select this spectrum because the wavelength of the 5200\AA feature, which was somewhat redder at earlier epochs, at this and later epochs coincides with that of the equivalent $[\text{Fe II}]$ feature in the nebular spectra

of SNe Ia (Axelrod 1980), indicating that other contributions (see Section 5) are now negligible. Table 3 gives the FWHM of our synthetic lines as a function of viewing angle. The corresponding observed value is 380\AA for the Fe-blend. This is estimated assuming that the continuum level is the value around 5700\AA where the flux has the minimum value.

The FWHM of the 5200\AA feature is narrower at this epoch than at earlier ones, and so is that of [O I]. While for the former feature other contributions may be responsible for a broader line at earlier epochs, in the case of [O I] the decreasing density of the outer envelope must be the principal reason. At late epochs the density of the outer envelope is expected to be too small to trap the γ -rays. Therefore we set the outermost velocity of the emitting region to reproduce the FWHM of the [O I] line (150\AA), and then calculate the profiles of the [Fe II] blend.

The [Fe II] and [O I] profiles for model C viewed at an angle of 15° from the jet direction and those for model F are compared to the observed spectrum of 26 Nov 1998 in Figure 4. For model F in Fig. 4, the outermost velocity of the emitting region is set to make the [Fe II] line as broad as possible, because for this model we cannot get a reasonable fit for the [O I] line, which is always much broader than the observation. Indeed, fitting the [O I] line was not possible for all models. Among the hypernova models, in a spherical explosion (model F) oxygen is located at higher velocities than iron, and the [O I] line is too broad for any choice of the outer velocity of the emitting region. This is because of the deficiency of oxygen with small velocity along the line of sight. Also, even though the Fe feature can be wider than the O line if O and Fe are mixed extensively, the expected ratio of the width of the Fe-blend and the O line even in a fully mixed model is $\sim 3 : 2$ (Mazzali et al. 2001). This is the result of taking blending into account, but giving all contributing lines the same intrinsic width. However, the observed ratio is even larger, $\gtrsim 2 : 1$, implying that the [Fe II] lines are intrinsically broader than the [O I] ones. Therefore the observed line profiles are not explained with a spherical hypernova model. The same is true for the moderately asymmetric model E viewed near the equator.

In our aspherical explosion models Fe is distributed preferentially along the jet direction, and so a larger ratio of the Fe and O line widths can be obtained. All the strongly aspherical hypernova models A, B and C, when viewed from a near-jet direction, give line widths comparable to the observed values. The very energetic model B cannot reproduce the O line when viewed near the equator, but this is because O is too fast near the equator and too depleted near the poles to give a low-velocity component.

When the degree of asphericity is high and the explosion is viewed from near the jet direction, the component lines in the [Fe II] blend have double-peaked profiles, the blue- and red-shifted peaks corresponding to matter situated in the two opposite lobes of the jet, where Fe is mostly produced. Because of the high velocity of Fe, the peaks are widely separated, and the blend is wide (Fig. 4, model C). In contrast, the [O I] line is narrower and has a sharper peak, because O is produced mostly in the r -direction, at lower velocities and with a less aspherical distribution.

Figure 5 shows the [O I] line for model C at different

orientations. The mean expansion velocity of O is lower in the aspherical cases than in the spherical model, because in aspherical models low-velocity, high-density O-dominated matter is found near the center (Fig. 3). Therefore the width of the O line in the aspherical models (A, C) viewed from near the equator can also be comparable to the observed width. This, however, does not mean that the line profile is always sharp as seen in SN1998bw. As shown in Figure 5, when the angle is large, the line first broadens, and eventually it develops two peaks. The reason can be seen in Figure 3. The highest density region has a typical velocity $\sim 3000 \text{ km s}^{-1}$ along the r -axis in this model. This corresponds to a Doppler shift of $\sim 120\text{\AA}$ between the approaching and receding parts when the SN is viewed from the r -direction. Therefore, to produce the narrow and sharply peaked O line in a hypernova model, the explosion must be aspherical and viewed from near the polar direction.

Figure 6 shows the profiles of the [Fe II] blend viewed at 5° for various aspherical hypernova models (A, B, C and E). In all of these models, the computed O line reproduces the observed one as discussed above. The Fe-blends appear to reproduce the 5200\AA feature reasonably well. The profiles show small peaks, which are not seen in the observations. These peaks are more pronounced in more asymmetric models. Mixing of the ejecta may distribute the ^{56}Ni to lower velocities, thus reducing the double-peaked profiles of the Fe lines. A spherical hypernova model (model F in Fig. 4) also gives a broad Fe line, and without the sharp peaks. However the O line is much too broad. Also, in this work we have used a spherical, uniform density nebular model to compute line emissivities. In an aspherical model, dense central and equatorial regions may have higher γ -ray trapping efficiency, which may result in stronger low-velocity line emission than in our model. Thus the component iron lines in the blend may have wider, flat-top profiles rather than double-peaked shapes, which could eliminate the minor peaks in the Fe blend seen in our present models. 2D γ -ray trapping calculations are therefore needed to compute the detailed spectra and the light curve.

It is reasonable to think that asphericity reduces the energy below that estimated previously based on spherically symmetric models. To examine this, we turn now to the lower energy explosion models (D, G). The [Fe II] and [O I] profiles for these models are shown in Figure 7. First of all, these models always give a narrower O line than the observed one. In these low energy models, in fact, the velocity of the ejecta is too small. The fastest-moving matter approaches the observer with a velocity of 3500 km s^{-1} for model G, and 5000 km s^{-1} in the case of the aspherical model (D) viewed from the z -direction. The observed FWHM (150\AA), however, indicates that there should be material moving faster than 7000 km s^{-1} . Also, because of the low velocity, the component [Fe II] lines are too narrow and do not blend to form a broad feature. From these arguments, we conclude that the explosion energy of SN1998bw should have been large, $E_K \sim 1 \times 10^{52} \text{ ergs}$.

5. CONCLUSION AND DISCUSSION

We calculated the nucleosynthesis in aspherical hypernova explosions. We find that in such explosions Fe is

mostly ejected at high velocity in a jet along the polar direction, while nearer the equatorial plane burning is less effective, and low-velocity O is mostly ejected. We show that the unusual ratio of the width of the O and Fe nebular lines in SN 1998bw can be explained with a strongly aspherical explosion model viewed from a near-jet direction. Also, in this case the O line has a very sharp peak, in agreement with the observations.

Much of our discussion was based on the identification of the 5200Å feature as a blend of [Fe II] lines. Although several caveats apply to that identification, because other lines may contribute, we claim that [Fe II] lines dominate. Other possible contributions are as follows. According to Sollerman et al. (2000) the feature contains not only [Fe II] lines but also lines of [Mg I], [O I] and possibly [Fe I]. Lines of [Mg I] are included in our nebular code, and the strength of the 5172Å emission, which is consistent with the 5470Å line reproducing the observed [Mg I] peak near 4500Å is much smaller than that of the [Fe II] lines. [O I] 5577Å is also included in our code, and it is strong and fills up the red part of the emission, but it does not contribute to the blue side (Mazzali et al. 2001). As for [Fe I], Sollerman et al. (2000) say that their models ‘have too low a degree of ionization’, suggest that the density in the Fe-emitting regions should be lower, and ‘regard the FeI emission as dubious’. We confirm this result.

Another possibility is allowed Fe II emission, such as identified by Filippenko (1989) in the Type II SNe 1987F and 1988I and by Filippenko et al. (1990) in the Type Ic SNe 1985F and 1987M. The main Fe II features are at 4570Å (multiplets 37 and 38), 5190Å (multiplet 42) and 5320Å (multiplets 42 and 43). These lines are not included in our atomic model, because not all the collision strengths for these transitions are available. In particular multiplet 42 is not available. However, several arguments apply against the Fe II identification in SN 1998bw. 1) In SNe 1987F and 1988I all three features are strong, while in the SNe 1985F and 1987M the feature at 4570Å is narrow and it is identified as [Mg I], suggesting that the feature at 5200Å could be [Fe II]. A similar situation holds for SN 1998bw, also a SN Ic. 2) Fe II emission occurs at high density. Filippenko (1989) infers $\log n_e \sim 9 - 10$ for SN 1987F. However, the densities we derive for SN 1998bw are more than one order of magnitude smaller (Mazzali et al. 2001). 3) The relatively low density is confirmed by the large ratio (~ 4) of the Ca II IR emission compared to [Ca II] 7300Å. Fig.2 of Ferland & Persson (1989) suggests that $\log n_e < 9$. Finally, the models of Mazzali et al. (2001), which are based on [Fe II] only, reproduce the 5200Å feature very well. In any case, extending the model to include Fe II lines is a worthwhile effort which we are going to make.

The 5200Å feature is bluer on Nov. 26 and thereafter than on earlier epochs. Two principal factors are probably responsible for that: 1) the disappearance of the continuum, which is still significant in the earlier spectra; 2) the reduced intensity of O I] 5577Å, as shown also in our models (Mazzali et al. 2001). This is a high-density line, and it decreases quickly in strength as the ejecta expand. Fading Fe II emission may also play a role in causing a small wavelength shift.

Weak unaccounted emission is present to the blue of the

[Fe II] feature (4800-5100Å). A similar emission is present in the nebular spectra of SNe Ia as well (Patat et al. 2001), and it is poorly reproduced by synthetic spectra. It may be due to a forest of weak [Fe II] and [Co II] transitions whose atomic parameters are not well known.

The [O I] line in other SNe Ib/c (Filippenko et al. 1995, Matheson et al. 2001) also shows a strongly peaked profile, as in SN 1998bw. This probably signals the existence of oxygen at low velocity in most SNe Ib/c. Although there are very few SNe Ib/c in which the feature centered at 5200Å is detected with enough S/N, it appears that in these objects the [O I] line has a similar profile. For low energy supernovae (1×10^{51} ergs), the spherical model G shows a sharply peaked [O I] line profile (Fig. 7). This seems to favor spherical explosions for these low energy supernovae. However, it is premature to conclude that asymmetry is completely absent in low energy SNIb/c, because the effects of asphericity in a late time spectra is not so large in case of normal supernovae as seen in Figure 7. This is due to the low expansion velocities. The oxygen line can be narrow even in the case of an aspherical explosion viewed from near the equator. For example, it is difficult to distinguish model D viewed from 75 deg from model G. Because the probability of viewing an aspherical SN from the near polar direction is smaller than it is to view it near the equator, the observations are not inconsistent with the possibility that most SNe Ib/c are more or less aspherical. More nebular spectra of SNe Ib/c with higher S/N ratio are needed for further investigation.

Our aspherical explosion models may be able to explain the slow decline of the late light curve of SN 1998bw. In these models, the equatorial region is denser than in a spherically symmetric model with the same explosion energy. At advanced epochs this region may be able to trap γ -rays more efficiently than a spherical model, as first suggested by Nakamura et al. (2001a). Chugai (2000) showed that a spherical model could reproduce the light curve, if the density near the center (i.e. in the Fe-dominated region) was increased above that of the hydrodynamical model of Iwamoto et al. (1998). However, Sollerman et al (2000) find that the O-dominated region should be dense, and the Fe-dominated region not dense. Although taken individually these conclusions are probably correct, they appear to be in conflict with one another. An aspherical model offers a natural solution, because it predicts the presence of high density, O-dominated matter near the center (Fig. 3).

A small degree of linear optical polarization ($\sim 0.5\%$) was reported in SN 1998bw (Kay et al. 1998; Iwamoto et al. 1998; Patat et al. 2001). This can be explained with different combinations of asphericity and viewing angle, or with large scale clumping in a basically spherical envelope. One solution is that ejecta with a moderate departure from sphericity are viewed from slightly off the axis of symmetry. Our strongly aspherical explosion model has an axis ratio of about 3:2 at the outer edge of the oxygen envelope (Fig. 3), therefore it is consistent with the observed polarization, if it is viewed from near the jet direction.

This work has been supported in part by the grant-in-Aid for COE Scientific Research (07CE2002, 12640233) of the Ministry of Education, Science, Culture, and Sports in Japan.

REFERENCES

- Axelrod, T.S., 1980, Ph.D. Thesis, UCRL5294, Lawrence Livermore National Laboratory
- Branch, D. 2001, in "Supernovae and Gamma Ray Bursts," eds. M. Livio, et al. (Cambridge: Cambridge University Press), 96
- Chugai, N.N., 2000, *Astronomy Letters*, 26, 797
- Ferland, G.J., & Persson, S.E., 1989, *ApJ* 347, 656
- Filippenko, A.V., 1989, *AJ* 97, 726
- Filippenko, A.V., Porter A.C., & Sargent W.L.W., 1990, *AJ*, 100, 1575
- Filippenko, A.V., et al., 1995, *ApJ* 450, L11
- Galama, T.J., et al. 1998, *Nature*, 395, 670
- Hachisu, I., Matsuda, T., Nomoto, K., & Shigeyama, T. 1992, *ApJ*, 390, 230
- Hachisu, I., Matsuda, T., Nomoto, K., & Shigeyama, T. 1994, *A&AS*, 104, 341
- Iwamoto, K., et al. 1998, *Nature*, 395, 672
- Kay, L.E., et al. , 1998, *IAU Circ.*, No.6969
- Khokhlov, A.M., Höflich, P.A., Oran, E.S., Wheeler, J.C., Wang, L., & Chtchelkanova, A.Yu. 1999, *ApJ*, 524, L107
- MacFadyen, A.I. & Woosley, S.E. 1999, *ApJ* 524, 262
- Matheson, T., Filippenko, A.V., Leonard, D.C., & Shields, J.C., 2001, *AJ* 121, 1648
- Mazzali, P.A., Nomoto, K., Patat, F., & Maeda, K. 2001, *ApJ*, 559, in press (astro-ph/0106095)
- Nagataki, S. 2000, *ApJS*, 127, 141
- Nakamura, T., Mazzali, P. A., Nomoto, K., & Iwamoto, K. 2001a, *ApJ*, 550, 991
- Nakamura, T., Umeda, H., Iwamoto, K., Nomoto, K., Hashimoto, M., Hix, R.W., & Thielemann, F.-K. 2001b, *ApJ*, 555, 880
- Nomoto, K., & Hashimoto, M. 1988, *Phys. Rep.*, 256, 173
- Nomoto, K., et al. 2001a, in "Supernovae and Gamma Ray Bursts," eds. M. Livio, et al. (Cambridge: Cambridge University Press), 144 (astro-ph/0003077)
- Nomoto, K., et al. 2001b, in "The influence of Binaries on Stellar Population Studies," ed. D. Vanbeveren (Kluwer), 507, (astro-ph/0105127)
- Paczynski, B. 1998, *ApJ*, 494, L45
- Patat, F., et al. 2001, *ApJ*, 555, 900
- Sollerman, J., Kozma, C., Fransson, C., Leibundgut, B., Lundqvist, P., Ryde, F., & Woudt, P. 2000, *ApJ* 537, L127
- Thielemann, F.-K., Nomoto, K., & Hashimoto, M. 1996, *ApJ*, 460, 408
- Woosley, S.E., Eastman, R.G., & Schmidt, B.P. 1999, *ApJ*, 516, 788
- Woosley, S.E. 1993, *ApJ*, 405, 273

¹² C	1.35E-01	¹³ C	1.84E-08	¹⁴ N	8.13E-05	¹⁵ N	2.63E-08	¹⁶ O	8.72
¹⁷ O	1.11E-07	¹⁸ O	1.77E-06	¹⁹ F	1.45E-09	²⁰ Ne	5.38E-01	²¹ Ne	1.92E-03
²² Ne	5.51E-02	²³ Na	1.87E-02	²⁴ Mg	3.35E-01	²⁵ Mg	4.08E-02	²⁶ Mg	8.86E-02
²⁶ Al	6.28E-05	²⁷ Al	7.06E-02	²⁸ Si	5.27E-01	²⁹ Si	5.43E-02	³⁰ Si	5.65E-02
³¹ P	7.09E-03	³² S	2.37E-01	³³ S	9.40E-04	³⁴ S	1.45E-02	³⁶ S	1.71E-05
³⁵ Cl	3.92E-04	³⁷ Cl	8.90E-05	³⁶ Ar	4.01E-02	³⁸ Ar	5.73E-03	⁴⁰ Ar	1.98E-07
³⁹ K	3.31E-04	⁴⁰ K	7.56E-08	⁴¹ K	2.30E-05	⁴⁰ Ca	3.57E-02	⁴² Ca	1.67E-04
⁴³ Ca	1.25E-05	⁴⁴ Ca	1.62E-03	⁴⁶ Ca	1.23E-09	⁴⁵ Sc	2.39E-06	⁴⁶ Ti	6.93E-05
⁴⁷ Ti	5.57E-05	⁴⁸ Ti	2.02E-03	⁴⁹ Ti	3.90E-05	⁵⁰ Ti	1.36E-09	⁵⁰ V	4.60E-09
⁵¹ V	9.91E-05	⁵⁰ Cr	4.39E-04	⁵² Cr	8.25E-03	⁵³ Cr	7.72E-04	⁵⁴ Cr	1.52E-07
⁵⁵ Mn	3.00E-03	⁵⁴ Fe	3.87E-02	⁵⁶ Fe	3.95E-01	⁵⁷ Fe	1.65E-02	⁵⁸ Fe	4.88E-08
⁵⁹ Co	6.56E-04	⁵⁸ Ni	2.71E-02	⁶⁰ Ni	1.20E-02	⁶¹ Ni	6.09E-04	⁶² Ni	5.08E-03
⁶⁴ Ni	4.29E-12	⁶³ Cu	1.80E-05	⁶⁵ Cu	1.12E-05	⁶⁴ Zn	1.60E-04	⁶⁶ Zn	8.93E-05
⁶⁷ Zn	6.53E-07	⁶⁸ Zn	1.23E-07	⁶⁹ Ga	9.72E-10	⁷¹ Ga	2.45E-10	⁷⁰ Ge	1.02E-09

TABLE 1

Detailed Yields of Model C (M_{\odot})

Species	[X/O] ^a	[X/Fe]	Species	[X/O]	[X/Fe]
¹² C	-1.31	-0.880	⁴⁰ Ca	-0.183	0.246
¹⁴ N	-4.09	-3.66	⁴⁴ Ca	0.0989	0.529
¹⁶ O	0.000	0.430	⁴⁵ Sc	-1.17	-0.740
¹⁹ F	-5.40	-4.97	⁴⁸ Ti	0.0153	0.445
²⁰ Ne	-0.437	-0.00731	⁵¹ V	-0.538	-0.109
²³ Na	-0.210	0.220	⁵² Cr	-0.215	0.215
²⁴ Mg	-0.146	0.284	⁵⁵ Mn	-0.605	-0.176
²⁷ Al	0.127	0.557	⁵⁴ Fe	-0.224	0.206
²⁸ Si	-0.0516	0.378	⁵⁶ Fe	-0.430	0.000
³¹ P	-0.0192	0.411	⁵⁹ Co	-0.668	-0.238
³² S	-0.182	0.248	⁵⁸ Ni	-0.220	0.210
³⁵ Cl	-0.769	-0.339	⁶³ Cu	-1.46	-1.03
³⁶ Ar	-0.244	0.186	⁶⁴ Zn	-0.750	-0.320
³⁹ K	-0.979	-0.549			

TABLE 2

Abundances of major stable isotopes relative to the solar values for Model C

^a[A/B] $\equiv \log_{10}(A/B) - \log_{10}(A/B)_{\odot}$

Model	α/β	$E/10^{51}$ ergs	E_K	fraction ^a	angle ^b [deg]	Fe FWHM ^c [Å]	O FWHM [Å]	outer velocity [km s ⁻¹]
A	16	10		0.65	5	376	150	9000
					15	344	150	8500
					30	304	150	8000
					45	248	150	6500
					60	216	150	5000
					75	144	150	4500
					85	144	150	4500
B	8	30		0.5	5	352	150	10000
					15	344	150	9500
					> 30		Too broad [O I]	
C	8	10		0.5	5	296	150	10000
					15	304	150	9500
					30	280	150	8500
					45	232	150	6500
					60	216	150	5000
					75	176	150	4500
					85	160	150	4000
D	8	1		0.5	5	224	80	5000
					15	216	80	5000
					30	216	72	5000
					45	200	80	5000
					60	192	80	5000
					75	160	88	5000
					85	128	88	5000
E	2	10		0.5	5	288	150	8500
					15	296	150	8000
					30	264	150	7000
					> 45		Too broad [O I]	
F	1	10		0.5			Too broad [O I]	
G	1	1		0.5	144	96		3500

TABLE 3

Half Line Widths

^aThe ratio of the kinetic energy to E initially deposited.^bAngle between the line of sight and the jet direction.^cHalf line widths of the [Fe II]-blend (near 5200Å) for SN 1998bw. The observed value is 380 Å.

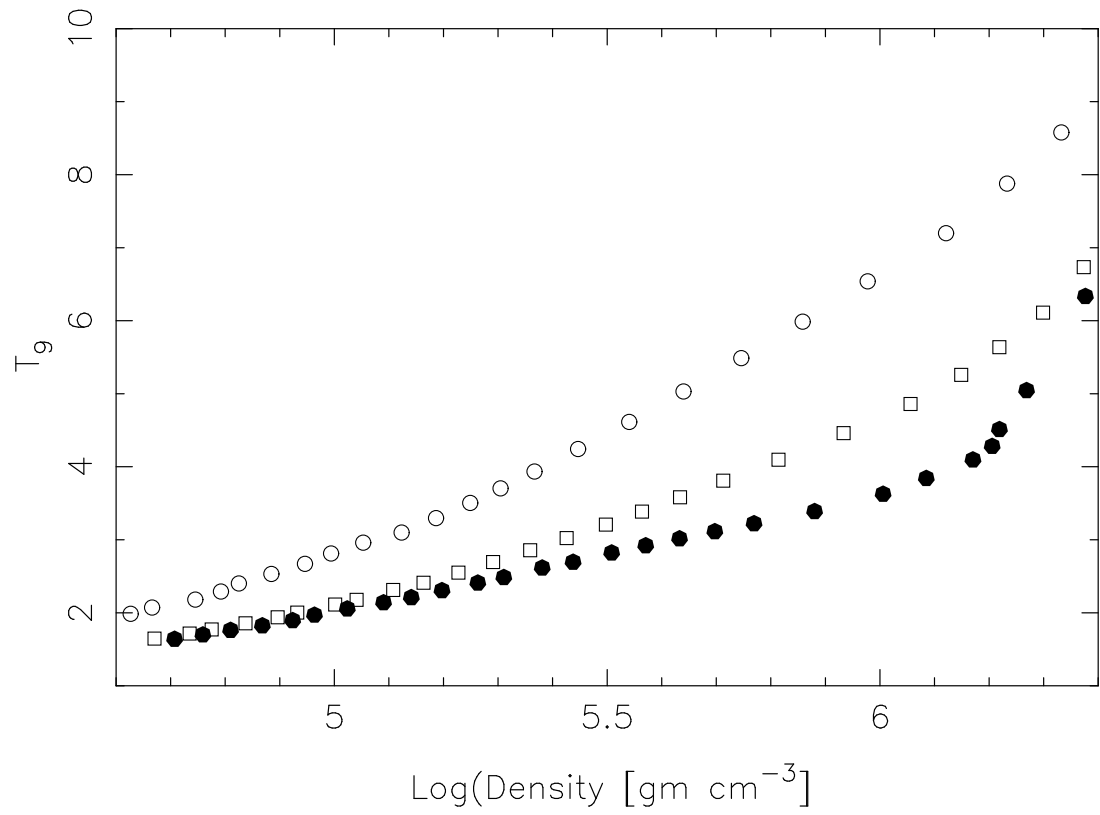


FIG. 1.— The $\rho - T$ conditions of individual test particles at their temperature maximum (where $T_9 \equiv T(\text{K})/10^9$). For model C, the open circles denote those along the z -axis, and the filled circles denote those along the r -axis. The open squares denote those of model F (spherical model).

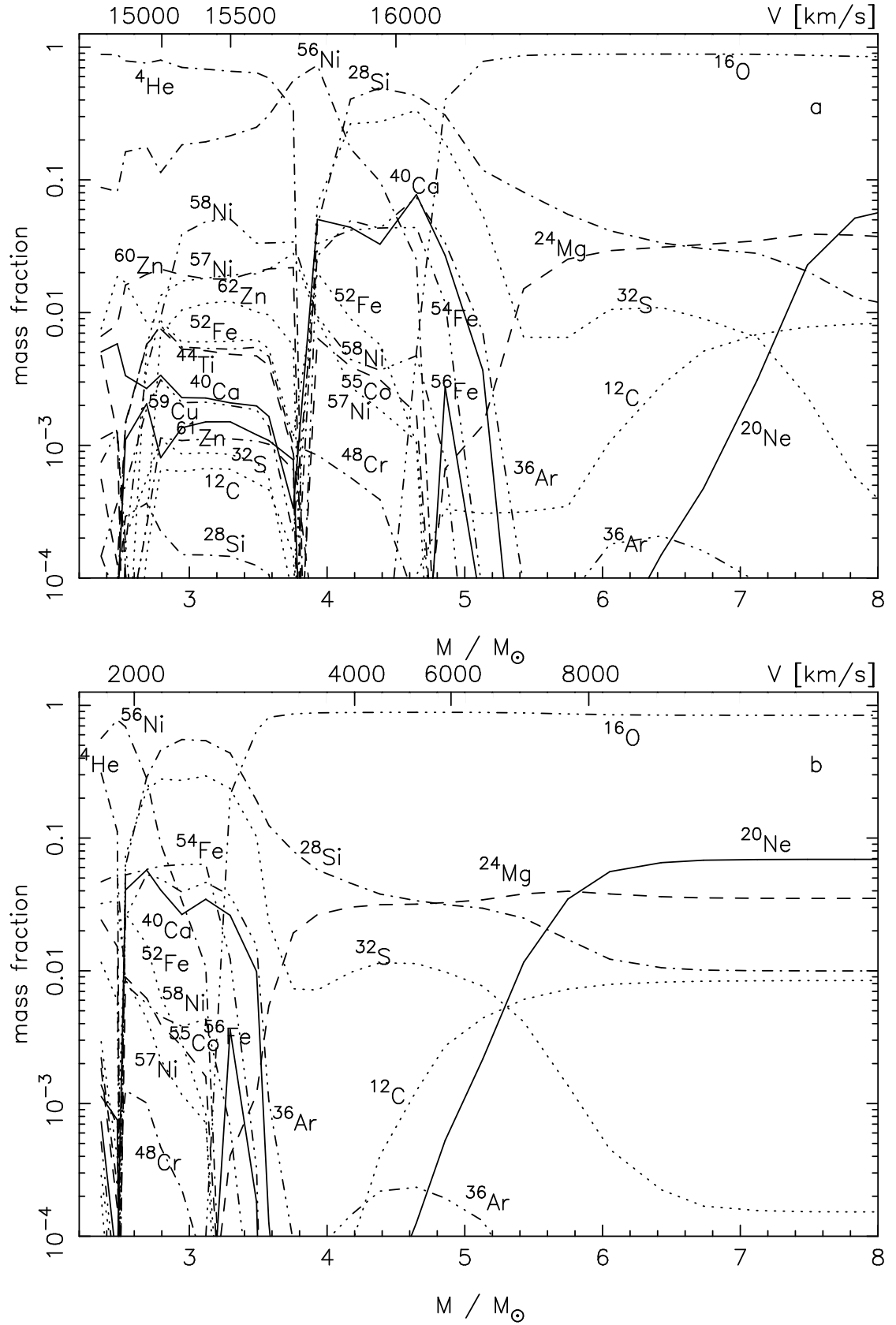


FIG. 2.— The isotopic composition of the ejecta of model C in the direction of the jet (upper panel) and perpendicular to the jet (lower panel). The ordinate indicates the initial spherical Lagrangian coordinate (M_r) of the test particles (lower scale), and the final expansion velocities (V) of those particles (upper scale).

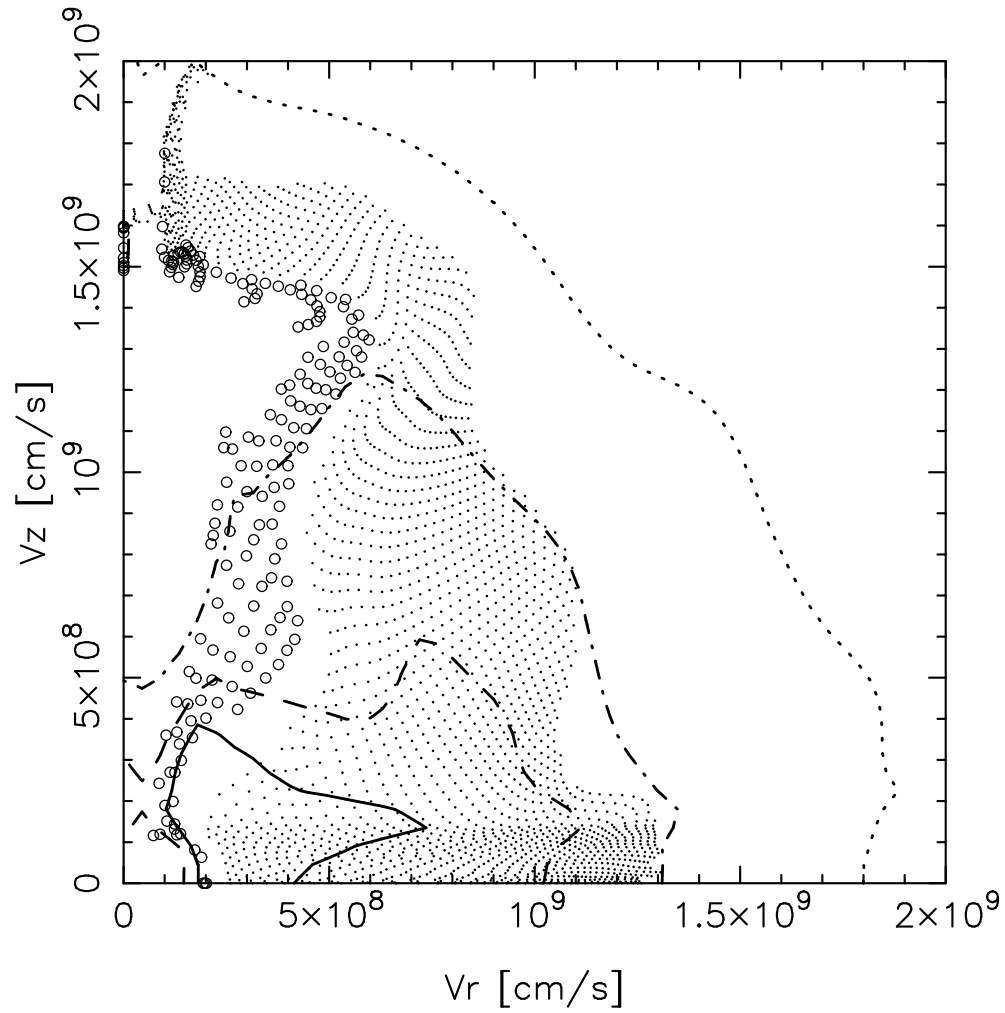


FIG. 3.— The 2D distribution of ^{56}Ni (open circles) and ^{16}O (dots) of model C in the homologous expansion phase. Open circles and dots denote test particles in which the mass fraction of ^{56}Ni and ^{16}O , respectively, exceeds 0.1. The lines are density contours at the level of 0.5 (solid), 0.3 (dashed), 0.1 (dash-dotted), and 0.01 (dotted) of the max density, respectively.

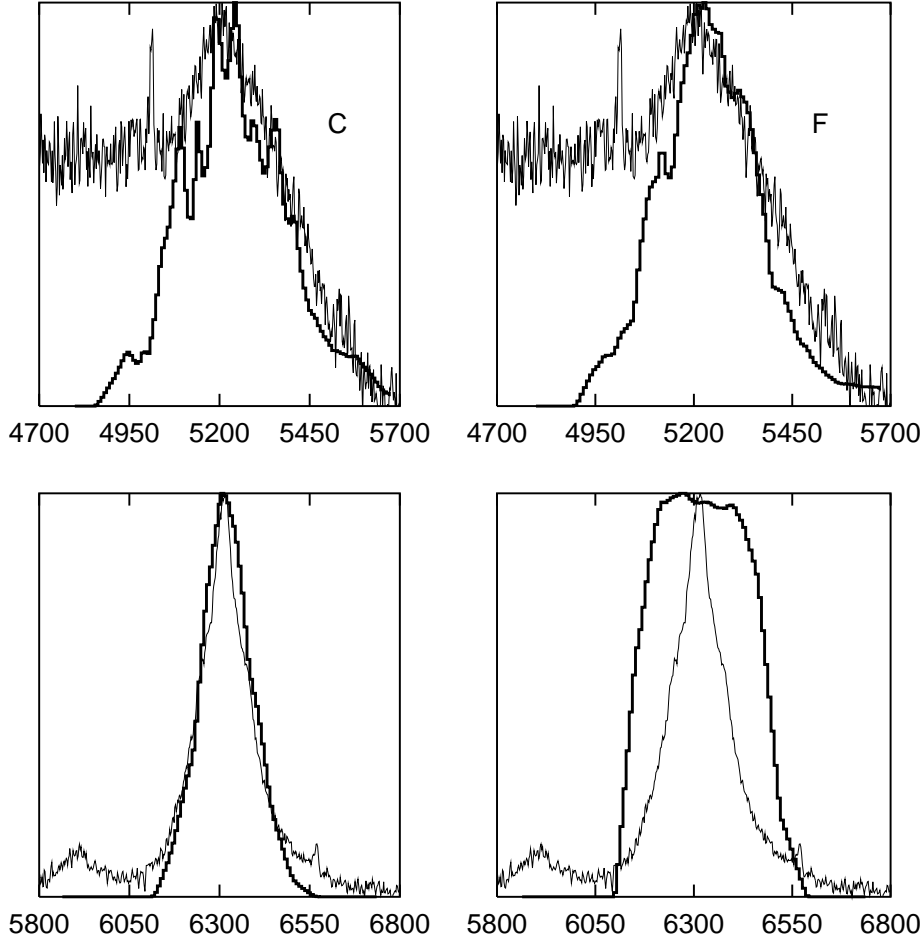


FIG. 4.— The profiles of the [Fe II] feature (upper panels) and of [O I] 6300, 6363 Å (lower panels) for model C viewed at 15° from the jet direction (left panels; thick lines) and for model F (right panels). The observed lines at a SN rest-frame epoch of 216 days are also plotted for comparison (thin lines, Patat et al. 2001). The intensities of the strongest lines, normalized to O I] 6300.3Å are: [Fe II] 5158.8Å: 0.122; [Fe II] 5220.1Å: 0.026; [Fe II] 5261.6Å: 0.083; [Fe II] 5273.3Å: 0.039; [Fe II] 5333.6Å: 0.060; [Fe III] 5270.4Å: 0.032; [O I] 5577.3Å: 0.022; and [O I] 6363.8Å: 0.330.

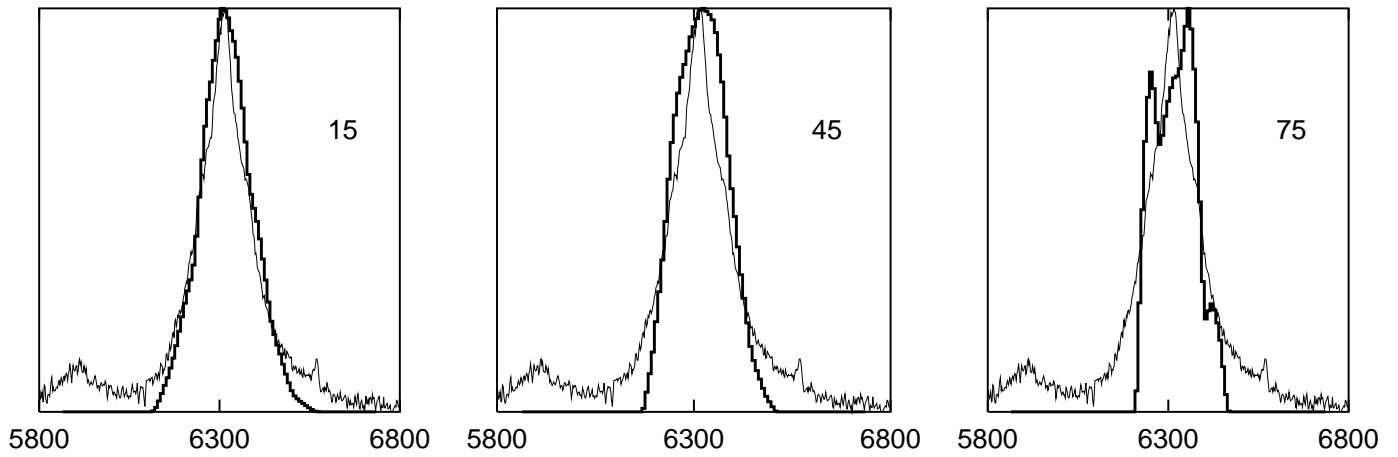


FIG. 5.— The profiles of [O I] 6300, 6363 Å for model C with different orientation. The angles between the observer and the z -axis are 15° (left), 45° (center) and 75° (right), respectively.

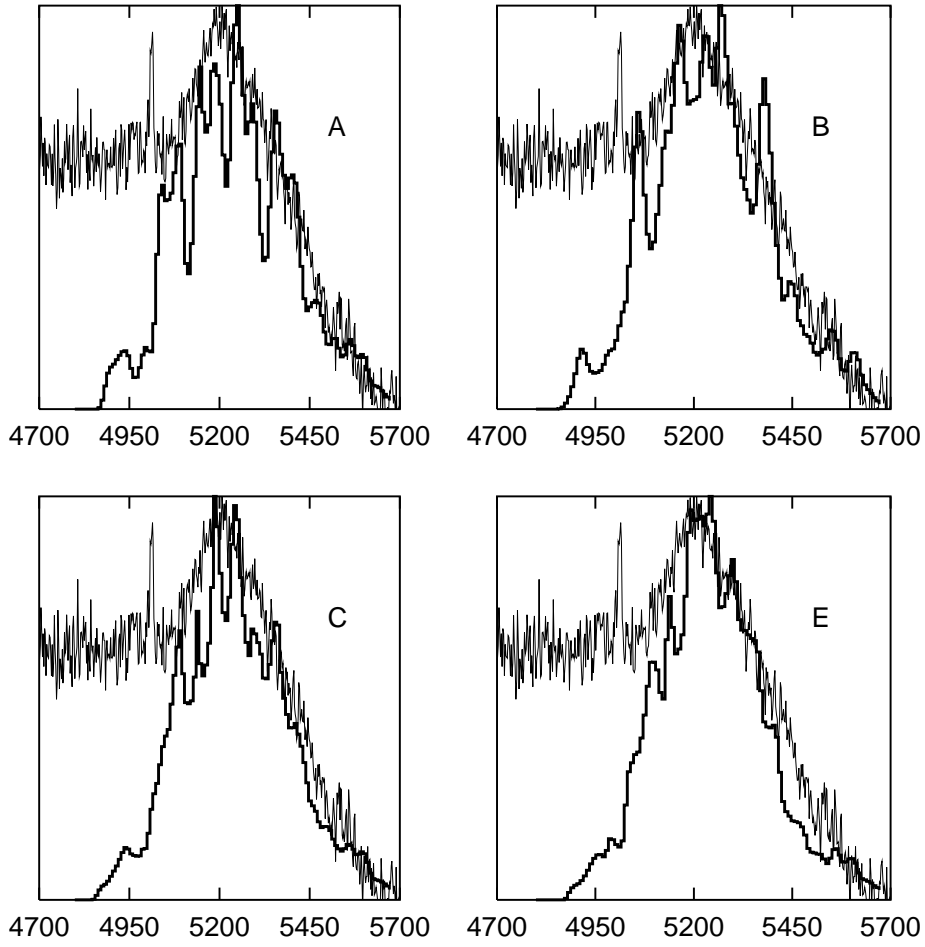


FIG. 6.— The profiles of the [Fe II] feature for hypernova models viewed at 5° . Each panel shows model A (upper-left), B (upper-right), C (lower-left), and E (lower-right), respectively.

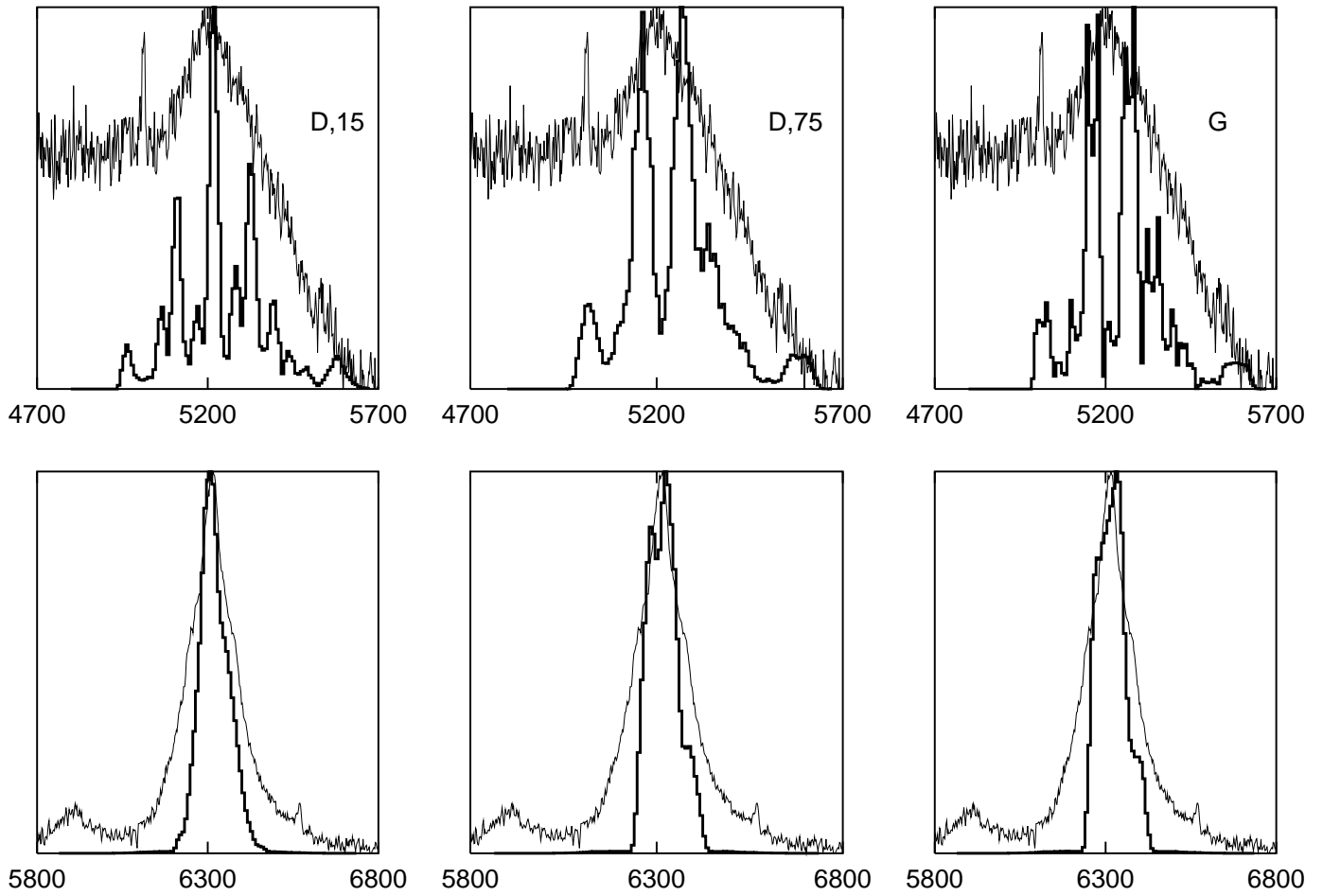


FIG. 7.— The profiles of the [Fe II] feature (upper) and the [O I] (lower) for normal energetic models. Those of model D viewed at 15° (left), 75° (center), and model G are shown.